

Shack-Hartmann Phasing of Segmented Telescopes: Systematic Effects from Lenslet Arrays

Mitchell Troy^a, Gary Chanan^b, and Jennifer Roberts^a

^aJet Propulsion Laboratory, California Institute of Technology, Pasadena, CA 91109

^bDepartment of Physics and Astronomy, University of California Irvine, Irvine, CA 92697

ABSTRACT

The segments in the Keck telescopes are routinely phased using a Shack-Hartmann wavefront sensor with subapertures that span adjacent segments. However, one potential limitation to the absolute accuracy of this technique is that it relies on a lenslet array (or a single lens plus a prism array) to form the subimages. These optics have the potential to introduce wavefront errors and stray reflections at the subaperture level that will bias the phasing measurement. We present laboratory data to quantify this effect, using measured errors from Keck and two other lenslet arrays. In addition, as part of the design of the Thirty Meter Telescope Alignment and Phasing System we present a preliminary investigation of a lenslet-free approach that relies on Fresnel diffraction to form the subimages at the CCD. Such a technique has several advantages, including the elimination of lenslet aberrations.

Keywords: Telescopes, Segmented Mirrors, Optical Alignment, Phasing

1. INTRODUCTION

The TMT Alignment and Phasing System¹ (APS) is responsible for the optical alignment and shape control of the TMT optics.² APS is a modified Shack-Hartmann camera modeled after the successful Keck Phasing Camera System³ (PCS). At Keck we phase the primary mirror by measuring interference effects between adjacent segments. At the re-imaged pupil, circular apertures are placed such that they straddle the edges between segments. The test then uses the details of the diffraction pattern formed by the interference between each half of the subaperture in order to determine the relative edge height between two adjacent segments.^{4,5} The subapertures on PCS are 120 mm in diameter at the primary mirror and APS will use the same size. The phasing procedure, unlike a traditional Shack-Hartmann test, uses high order information in the diffraction pattern, not just the centroid location, and as a result the image quality of the lenslets is critical.

Because of problems with lenslet image quality, PCS used an array of prisms in place of the usual lenslet array. The prisms were of very high optical quality and this substitution worked very well. (The focusing power normally associated with lenslets was provided by a single downstream macroscopic lens.) However, the much larger number of intersegment edges (1386 vs 84) on TMT, combined with the greater pupil demagnification (400 vs. 200), makes it impractical to build prism arrays of the appropriate geometry. (The individual prisms would have to be half the size of the 2 mm × 3 mm prisms used in PCS.) In the twenty years since PCS was designed lenslet manufacturing techniques have improved significantly.

In order to quantify the impact on phasing from lenslet arrays we have purchased a set of lenslet arrays manufactured via photolithography as described in Section 2. In Section 3 we describe the optical testbed used to investigate the lenslet image quality. In Section 4 we describe our results from characterization of these lenslets. In Section 4.5 we discuss the phasing results of the photolithography lenslets, epoxy replica lenslets and the PCS prisms. We then briefly discuss an alternate approach for phasing that does not use lenslets at all in Section 5. Finally, in Section 6 we summarize our conclusions and provide suggestions for future work.

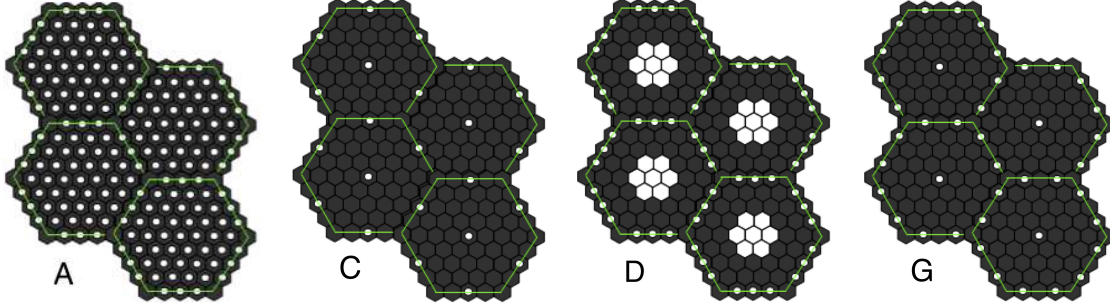


Figure 1. Examples of masks A, C, D, and G. Green lines represent telescope segments. All apertures (white areas) on the green lines are $300\mu\text{m}$ for phasing and the interior apertures are either $400\mu\text{m}$ (A, C, G) or unmasked (D) for Shack-Hartmann measurements.

2. LENSLET ARRAYS

The lenslet arrays for the testbed are designed to the same specifications (pitch, focal length and lenslet aperture sizes) as the arrays from the APS conceptual design study^{.1} The detailed specifications are show in Table 1. Opaque masks (Figure 1) are applied to the lenslet arrays to define the required apertures for phasing as well as to control the effects due to diffraction from the edges of the individual lenslets.

Mask A would allow operation of all modes of APS (Shack-Hartmann over the full segment and phasing), however crowding of the spots may adversely affect phasing and centroiding. At the time these lenslet arrays were purchased the baseline APS design had a 4K by 4K pixel detector and 37 Shack-Hartmann spots internal to each segment. However, based on analysis of warping harness performance⁶ the design now has a 9K by 9K pixel detector and as many as 127 Shack-Hartmann spots internal to each segment. Mask C would provide the basic APS phasing mode with minimal effects from adjacent spots. This is the baseline mask for the testbed. Masks D and G allow testing of 2-spot and 3-spot phasing, respectively, without the crowding effects from the interior spots. In addition, Mask D tests the effects of no mask to determine if the diffraction and wavefront error induced at lenslet boundaries are significant. Figure 2 shows a small portion (~ 5 mm) of the subimage pattern corresponding to each lenslet array/mask for comparison to Figure 1.

Table 1. Specifications of the lenslets used in the testbed.

| | |
|--|-------------------------------|
| Lenslet type | Spherical Plano-Convex |
| Lenslet aperture type | Hexagonal with circular masks |
| Lenslet packing | Hexagonal |
| Lenslet fill factor | $>95\%$ |
| Lenslet aperture | $446 \mu\text{m}$ |
| Lens to lens pitch | $446 \pm 1.0 \mu\text{m}$ |
| Focal length | 45 mm |
| Focal length variations between lenslets | 5% |

3. DESCRIPTION OF OPTICAL TESTBED

The goal of the testbed is to characterize the lenslet arrays and to test their functionality for phasing and Shack-Hartmann measurements. A simple optical setup is important for lenslet characterization, so the basic testbed consists of a fiber coupled source, a collimating lens, the lenslet array and an Apogee U47 1K by 1K pixel CCD with $13\mu\text{m}$ pixels (Figures 3 and 4). With no relay optics between the lenslet and the CCD, the plate scale is

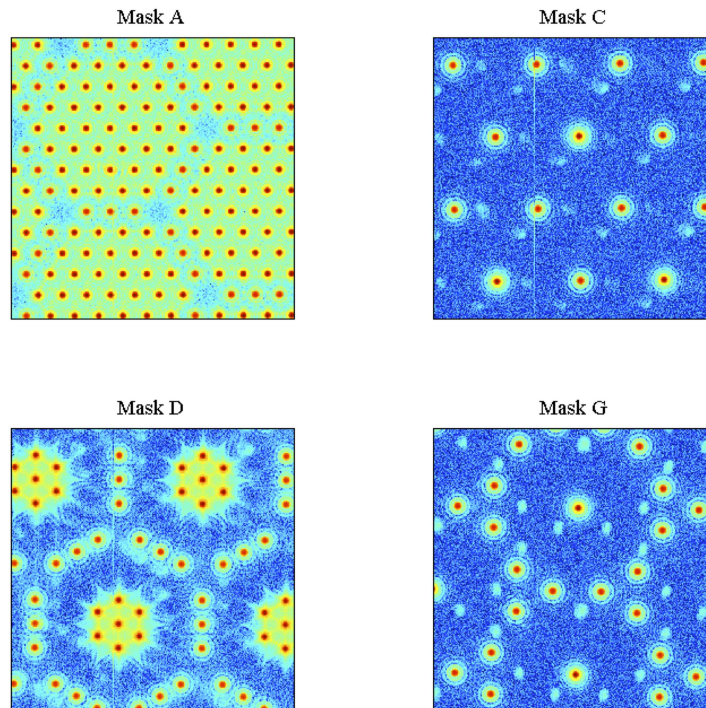


Figure 2. Small portions (~ 5 mm) of the subimage patterns corresponding to the various masks, illuminated at 600 nm (logarithmic scale).

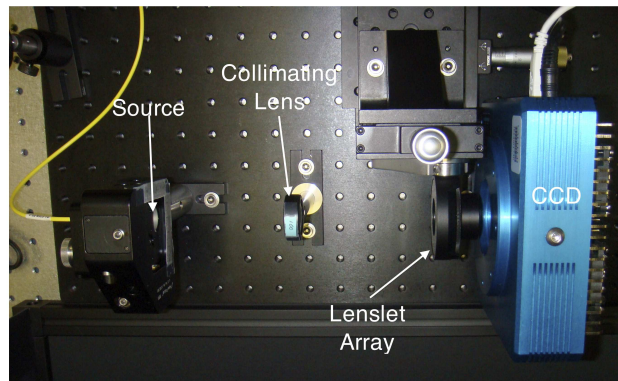


Figure 3. The testbed setup.

0.149 arcseconds/pixel, which is the same as PCS, but slightly better sampled than the original APS conceptual design, which has 0.21 arcseconds/pixel.

The light source is a single mode fiber-coupled tungsten-halogen source with space for filters. The fiber is held in a 5-axis mount, which allows for fine alignment and provides x-y-z translation to test Shack-Hartmann measurements of tip/tilt and focus. The light is collimated by a 100 mm EFL, AR-coated achromat. The lenslet array is placed with the flat side first to minimize the effect of the substrate on the wavefront. Spherical aberration from individual lenslets due to this orientation is negligible compared to diffraction effects. The lenslet array has x-y-z translation as well as rotation for fine alignment to the CCD and to scan the whole array. With

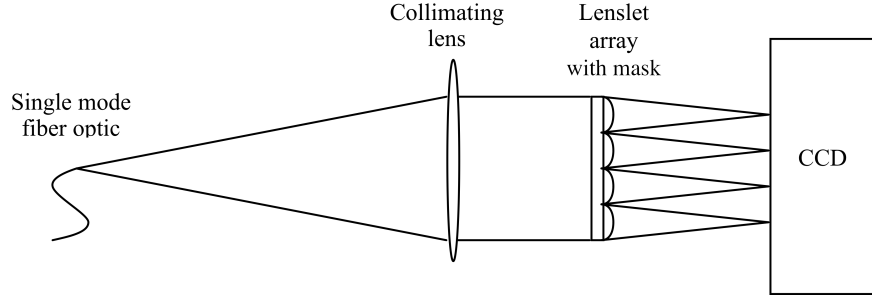


Figure 4. Optical setup of the APS lenslet testbed.

no relay optics between the lenslet and the CCD only about 75% of the array is imaged at one time. The CCD is placed at the geometrical focus of the lenslets. Most of the data were taken using narrowband (10 nm bandpass) filters in the source at 600, 800 and 900 nm. These cover the wavelength range for the APS instrument. All exposures were 5 seconds long.

The source collimation was verified with a shear plate. The lenslet-to-CCD distance was set using Shack-Hartmann measurements of a known tilt, created by translating the source. See Section 4.3 for further details.

4. ANALYSIS OF PHOTOLITHOGRAPHY LENSLETS

4.1. Spot Size

Table 2 shows the FWHM of the subimages for each of the 2 aperture sizes. The variation in size is on the order of 0.5%. The measured spot size values are a better fit to slightly larger apertures for both of the aperture types, $317\mu\text{m}$ and $410\mu\text{m}$. Scans of each array show that there are no visible defects, although dust particles can have a significant effect.

Table 2. Spot size (FWHM) and uniformity of the lenslet arrays. The variation in size is on the order of 0.5%.

| | Wavelength | 600 nm | 800 nm | 900 nm |
|----------------------------|------------|----------------------------|-----------------------------|-----------------------------|
| 300 μm aperture | Predicted | 93 μm | 124 μm | 139 μm |
| | Measured | $89.5 \pm 0.2 \mu\text{m}$ | $116.8 \pm 0.3 \mu\text{m}$ | $131.1 \pm 0.4 \mu\text{m}$ |
| 400 μm aperture | Predicted | 70 μm | 93 μm | 104 μm |
| | Measured | $69.5 \pm 0.4 \mu\text{m}$ | $90.5 \pm 0.5 \mu\text{m}$ | $100.5 \pm 0.4 \mu\text{m}$ |

4.2. Reflections

The images of the spots from the lenslet arrays exhibit what appear to be reflections (see Figure 5). The reflections duplicate the pattern of the arrays clear aperture, offset from the main pattern by 0.8 to 1 mm. There is a strong wavelength dependence to the reflections. The flux in the additional images at 900 nm is 3-5% of the main images, but at 600 nm the reflections are only 0.3-0.5% of the main images. Reflections from the camera window were ruled out as the cause by replacing the lenslet array with a 45 mm lens. Reflections from the source optics were ruled out by replacing the source fiber with one that was angle polished, since the only reflective surface in the source is the fiber tip. When the lenslet piece is rotated, the reflected pattern also rotates.

The most likely explanation is that the reflections come from the array itself. To produce the observed effect, the array pieces would have to have a wedge on the order of 0.5 deg. There would also have to be no AR coating on the lenslet side and the backside of the chrome mask would have to be highly reflective at 900 nm. The

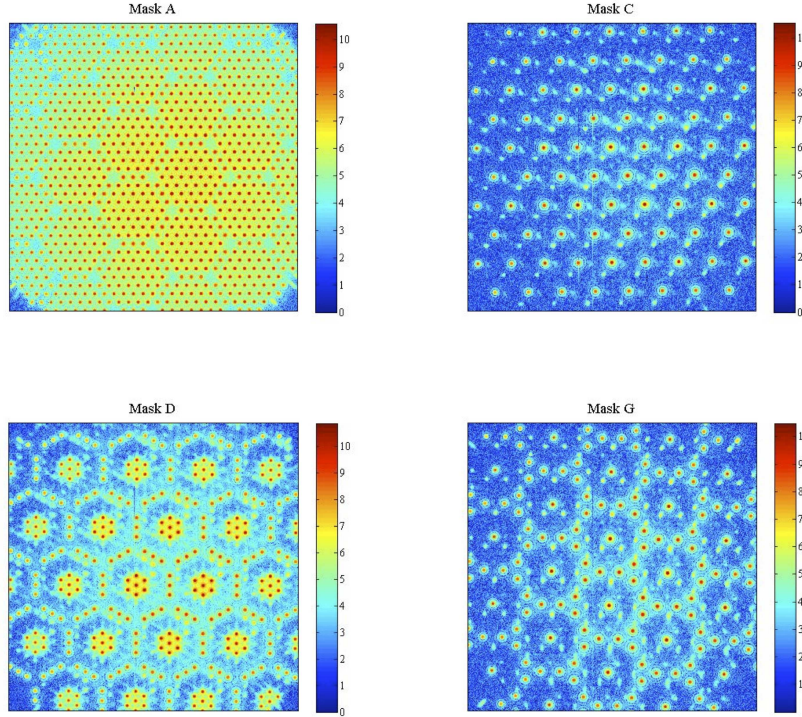


Figure 5. Images from each array at 900 nm, log scaled. Red spots are the main images, green/yellow spots are the reflections. Reflections are most prominent in Mask C and Mask G, the arrays with the highest proportion of masked area to clear aperture. The images are plotted on a logarithmic scale in order to reveal the reflections more clearly.

vendor stated that the lenslet was AR coated, however, it is not clear which side is AR coated. The vendor also provided mask reflectivity measurements, however it is not clear if these apply to the back or front surface of the mask. The mask does appear to be much more reflective from the back surface than the front surface, based on a visual inspection. If the wedge were smaller, the light would not reflect off the mask, but rather go through the aperture in the mask. Therefore, reducing the wedge to a few arcminutes or less should solve the problem. More information is required from the vendor to determine if the wedge can be better controlled and what other options there are for the opaque mask. If none of these options reduces the reflections sufficiently, it may be possible to manufacture a separate opaque mask that has diffuse scattering and align it to the lenslets separately.

4.3. Shack-Hartmann Verification

For Shack-Hartmann measurements, the important parameter is the distance from the lenslet array to the detector. This determines the amount of spot motion for a given tilt across a lenslet. In order to test the Shack-Hartmann operation of the system, a tilt was introduced by translating the source in x and y . Three full turns of the source coarse actuator translates the source by $951 \mu\text{m}$, which, for the 100 mm EFL collimating lens, gives 32.7 arcmin of tilt at the lenslet array. For the APS design, this corresponds to 4.8 arcsec on the sky.

The measured motions for X and Y in both directions are given in Table 3 along with the measurement uncertainties from the centroid calculations. The expected spot motion at the CCD is ± 32.9 pixels which agrees with the observed value to about $\pm 0.2\%$. The error in the ability to produce the desired tilt, due to uncertainty in the actuator position, was determined by returning to center after each measurement. The repeatability of this motion was ± 0.3 pixels; however the uncertainty was larger in the x -direction due to awkward placement of

the actuator. A more accurate method of introducing tilt will be required for calibration of the actual system, but this verifies the basic functionality and centroiding accuracy.

Table 3. The measured spot motion for the equivalent of 4.8 arcsec of tilt at the telescope

| | | |
|-------------------|------------|-------------|
| X Motion (pixels) | 32.28±0.06 | -33.31±0.06 |
| Y Motion (pixels) | 33.51±0.06 | -32.97±0.05 |

4.4. Pitch Between Spots

In order to verify the pitch of the lenslets we calculated the centroids via a Gaussian fit of all of the segment center (400 μm diameter) lenslets for Mask C at 600, 800 and 900 nm. A total of 21 lenslets were used in the calculation for each wavelength and the distance between nearest neighbors was calculated. The expected distance between spots is $12/\sqrt{3}$ times the lenslet pitch. Table 4 shows the lenslet pitch calculated for the 3 different wavelengths. The results are consistent with the specifications, which called for a lenslet pitch of $446.0\pm 1.0\mu\text{m}$.

Table 4. The measured pitch of the SUSS lenslet array is consistent with the specification of $446.0\pm 1.0\mu\text{m}$.

| Wavelength | Measured lenslet pitch |
|------------|--------------------------|
| 600 nm | 446.2±0.07 μm |
| 800 nm | 445.8±0.06 μm |
| 900 nm | 445.9±0.08 μm |

4.5. Phasing Quality

In this section we look at the “edge” lenslets (300 μm diameter) in Mask C at three different wavelengths to investigate the impact on phasing measurements due to the lenslet array itself. In future work we will look at the impact of image crowding. In the following we describe the data we collected, how the analysis was conducted, present the results, and discuss potential future work.

We analyzed the subimage pattern corresponding to Mask C at wavelengths of 600, 800 and 900 nm with a 10 nm bandpass filter. Data were taken with the lenslet in a nominal position and with the lenslet translated up, down, left and right by 100 μm . Ten frames of data were taken at each of the 5 lenslet positions for each wavelength. The frames were background subtracted and a correction was applied for three bad columns in the CCD. The bad CCD columns were simply corrected by replacing them with the average of the columns on the left and right of the bad column. All subimages in the CCD frame were found and the two different size lenslets were sorted by looking at the subimage FWHM. In addition only subimages in the central 700 by 700 pixels of the CCD were considered for analysis to avoid potential problems with vignetting in the optics. Figure 6 shows an example of one of the images, with boxes drawn around the 33 subimages used in the phasing analysis.

The phasing data analysis follows the same basic algorithm as used in the Keck Phasing Camera.⁵ The nominal testbed pixel scale is 0.149 arcseconds/pixel on the sky. The cross correlations were performed over a 4.9 by 4.9 arcsecond box of data (33 by 33 pixels) consistent with what is used in PCS. The nominal mask size at the TMT pupil is 120 mm.

The actual data processing is similar to PCS with two exceptions. The first involves the centroiding algorithm. The phasing results are very sensitive to the centroiding accuracy and the simpler centroiding algorithm used in the present analysis may be introducing some increased phasing measurement noise and/or bias. A second difference is that instead of using 11 phasing templates to cross correlate against we used 33. Simulations were conducted at a wavelength of 900 nm and without the cross hairs that nominally mask out the segment gaps.

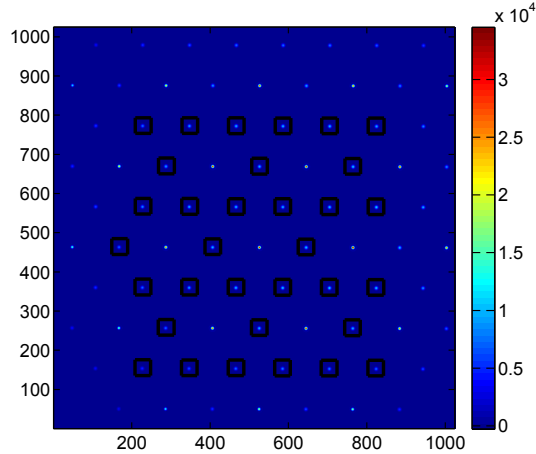


Figure 6. The subimage pattern corresponding to Mask C, plotted with a linear stretch. The black boxes indicate the subimages used in the calculation of phase errors.

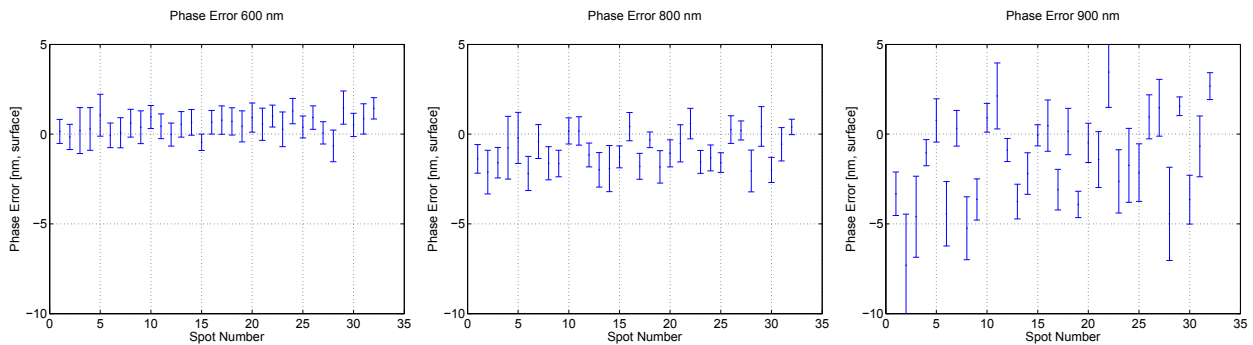


Figure 7. The phase errors (surface) calculated at 600, 800 and 900 nm for each of the spots indicated in Figure 6. The error bars on each data point are set by the 50 measurements taken at 5 different lenslet positions and represent ± 1 standard deviation.

The 33 phasing templates reduce the Peak-to-Valley (PV) error from 26.2 nm to 3.2 nm over the full $\pm\lambda/4$ range of piston errors. However, over the limited range of phasing errors investigated in this report ($\sim \pm 20$ nm) the RMS error from using 11 or 33 templates is the same (0.6 nm), so this change likely had no impact on the results.

We collected a total of 50 frames of data (over 5 different lenslet translations) for each wavelength. This provides 50 measurements of the nominally null phase of each lenslet at each wavelength. A plot of the mean and standard deviation of the phase error for each lenslet is shown for wavelengths of 600, 800 and 900 nm in Figure 7. Table 5 shows the RMS and PV of the mean phase error, as well as the average measurement error. The mean phase error in each filter (Table 5, column 2) is non-zero; this may indicate a model mismatch, a bias in the centroiding algorithm, or potentially a bias from the reflections (which get stronger at the longer wavelengths). To be conservative we calculate the RSS phase error to include the impact of this non-zero mean error. At a wavelength of 600 nm the measured phase errors are consistent with the measurement noise so we can only conclude that the phase errors from the lenslets are less than ~ 1 nm. At a wavelength of 900 nm the RMS phase error is 2.92 nm, or twice the measurement error.

The Keck PCS produces phase errors with an RSS of 1.86 nm and a PV of 16 nm at a wavelength of 605 nm when measured using a fiber at the focus of the system. The PCS prisms include cross hairs which do not exist on the photolithography lenslets. A set of epoxy replica lenslets were also tested at 605 nm with cross hairs from an external mask and had an RMS error of 4.50 nm and PV of 17 nm.

Table 5. A summary of the phasing errors obtained with Mask C.

| Wavelength (nm) | Mean phase error (nm, surface) | RMS Phase error (nm, surface) | Peak-to-Valley of error) (nm, surface) | Average measurement noise (nm, surface) | Mean cross correlation coefficient |
|--------------------|--------------------------------------|-------------------------------------|---|---|---------------------------------------|
| 600 | 0.51 | 0.71 | 2.14 | 0.78 | 0.9993 |
| 800 | -0.94 | 1.31 | 2.78 | 0.86 | 0.9998 |
| 900 | -1.43 | 2.92 | 10.8 | 1.38 | 0.9995 |

The results of tests from various phasing sensors and lenslet arrays are summarized in Table 6. We conclude that the photolithography lenslet array image quality tested for APS is consistent with that achieved with the PCS prisms and will not add significant systematic errors in the phasing of TMT.

Table 6. Summary of phase errors from various phasing sensors and lenslet arrays.

| System | Wavelength (nm) | RMS phase error (nm, surface) | Peak-to-Valley of error (nm, surface) | Average measurement noise (nm, surface) |
|----------------------|--------------------|-------------------------------------|---|---|
| PCS-prisms | 605 | 1.86 | 16 | No Data |
| Epoxy Replica | 605 | 4.50 | 17 | No Data |
| APS-photolithography | 600 | 0.71 | 2.14 | 0.78 |
| APS-photolithography | 900 | 2.92 | 10.8 | 1.38 |

5. FRESNEL DIFFRACTION

In systems with lenslets, the Fresnel number is $a^2/(\lambda F)$, where a is the aperture radius, λ is the wavelength and F is the focal length of the lenslet. The actual APS lenslets will be similar to those in the testbed, but will be stopped down to a diameter of $300 \mu\text{m}$. The resulting Fresnel number at a wavelength of 900 nm is 0.6 . For such small Fresnel numbers the maximum on-axis intensity of the diffraction pattern does not occur in the focal plane, but rather significantly in front of the focal plane.⁷ However, in our application, we are not trying to maximize the peak intensity, but rather to produce the desired diffraction pattern at the chosen image scale. Note that the intensity distribution in the focal plane is given correctly by Fraunhofer diffraction, independent of the Fresnel number of the lenslets. Therefore, it is important to align the system (as described in Section 4.3) by adjusting the lenslet-CCD distance to give the correct image scale, not to give the maximum on-axis intensity.

Although the Fresnel number of the lenslets is not relevant to the above considerations, it may be possible to exploit the low Fresnel number of the APS system by eliminating the lenslets entirely, leaving just a mask to define the subapertures. For an empty aperture, the Fresnel number is calculated as before, except that F is now the effective focal length of the system, which is simply equal to the mask-CCD distance. As the Fresnel number of the system goes to zero, one recovers the Fraunhofer diffraction pattern without the benefit of a lens. Figure 8 shows that for the chosen Fresnel number of 0.6 the differences between Fresnel and Fraunhofer diffraction are small, for both in phase and out of phase segments. There are several potential advantages to the lensless approach, including:

1. The problem of lenslet aberrations (which can introduce phasing errors or biases) is eliminated.
2. The problem of mask-lenslet registration is eliminated.

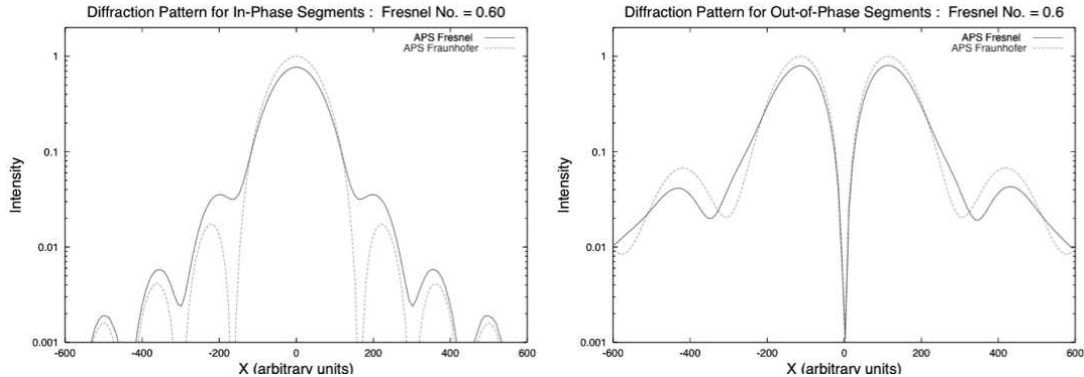


Figure 8. One dimensional cut through the diffraction pattern formed from in-phase (left plot) and a quarter wave (surface) out of phase (right plot) segments, calculated using a lens to form an image at the focal plane (Fraunhofer diffraction) and using just a mask at the pupil plane (Fresnel diffraction). At this Fresnel number, the lenslets have very little effect.

3. The problem of reflections from the lenslet surfaces is eliminated.
4. Fabrication problems associated with the irregular hexagonal pattern of the lenslets are eliminated.
5. There may be significant cost savings.

We plan to further investigate the lensless option in future work. If the nominal Fresnel number of 0.6 is not sufficiently small, it may be possible to reduce it with a modest design change of the APS optical system.

6. CONCLUSIONS

We have shown that the photolithography lenslet arrays appear adequate for phasing of the TMT telescope in terms of phase errors introduced from image quality of the lenslets. The only significant deficiency was that associated with reflections, as described in Section 4.2. However, as noted, there are several possible solutions. Further investigation is also needed to insure that the lenslets (and/or masks) can be manufactured on a non-uniform array, as the projected TMT pupil is non-uniform.

We have also shown that it may be possible to phase without any lenslet arrays, using just a mask and the effects from Fresnel propagation. As discussed in Section 5 there are several significant advantages to this approach. We will continue investigation in this area with both simulations and laboratory tests.

ACKNOWLEDGMENTS

This research was carried out in part at the Jet Propulsion Laboratory, California Institute of Technology, and was sponsored by the California Institute of Technology and the National Aeronautics and Space Administration. The TMT Project gratefully acknowledges the support of the TMT partner institutions. They are the Association of Canadian Universities for Research in Astronomy (ACURA), the California Institute of Technology and the University of California. This work was supported as well by the Gordon and Betty Moore Foundation, the Canada Foundation for Innovation, the Ontario Ministry of Research and Innovation, the National Research Council of Canada, the Natural Sciences and Engineering Research Council of Canada, the British Columbia Knowledge Development Fund, the Association of Universities for Research in Astronomy (AURA) and the U.S. National Science Foundation.

REFERENCES

1. M. Troy, G. Chanan, S. Michaels, R. Bartos, G. Bothwell, A. Give'on, R. Hein, M. Radin, J. Roberts, J. M. Rodgers, L. M. Scherr, B.-J. Seo, and D. Zimmerman, "A conceptual design for the thirty meter telescope alignment and phasing system," in *Ground-based and Airborne Telescopes II.*, L. Stepp, ed., *Ground-based and Airborne Telescopes II. Edited by Stepp* **7012**, p. 32, SPIE, 2008.
2. L. M. Stepp and S. E. Strom, "The Thirty-Meter Telescope project design and development phase," in *Second Backaskog Workshop on Extremely Large Telescopes*, L. A. Ardeberg and T. Andersen, eds., **5382**, pp. 67–75, SPIE, 2004.
3. G. A. Chanan, J. Nelson, T. Mast, P. Wizinowich, and B. Schaefer, "The W. M. Keck Telescope phasing camera system," in *Instrumentation in Astronomy VIII*, D. L. Crawford and E. R. Craine, eds., **2198**, pp. 1139–1150, SPIE, 1994.
4. G. A. Chanan, M. Troy, F. G. Dekens, S. Michaels, J. Nelson, T. Mast, and D. Kirkman, "Phasing the mirror segments of the Keck Telescopes: the broadband phasing algorithm," *Applied Optics* **37**, pp. 140–155, Jan. 1998.
5. G. A. Chanan, C. Ohara, and M. Troy, "Phasing the mirror segments of the Keck telescopes II: The narrow-band phasing algorithm," *Applied Optics* **39**, pp. 4706–4714, Sept. 2000.
6. B.-J. Seo, C. Nissly, G. Angeli, D. MacMynowski, N. Sigrist, M. Troy, and E. Williams, "Investigation of primary mirror segment's residual errors for the thirty meter telescope," in *Optical Modeling and Performance Predictions IV.*, Kahan, ed., **7427**, p. 14, SPIE, 2009.
7. Y. Li and E. Wolf, "Three-dimensional intensity distribution near the focus in systems of different fresnel numbers," *Journal of the Optical Society of America A: Optics* **1**, p. 801, Aug 1984.